Magn Reson Med Sci 2020; 19; 259–267
doi:10.2463/mrms.tn.2019-0052
Published Online: August 2, 2019

TECHNICAL NOTE

Novel Technique for Growth Plate Analysis Based on the Superposition of T_1- and T_2-weighted MR Imaging of Adolescent Wrists

Rafał Obuchowicz[1*], Andrzej Urbanik[1], and Adam Piórkowski[2]

In this article, a new method of information extraction on the basis of the differentiation of T_1- and T_2-weighted MR images is proposed. It relies on a technique of superposition of T_1- and T_2-weighted MR images with use of statistical dominance algorithm. On the basis of implemented image analysis, a reproducible extraction of growth zone of adolescent boys' wrists is possible.

Keywords: *bone age, children, magnetic resonance, statistical dominance algorithm*

Introduction

Growth of the long bones is traditionally evaluated by means of radiographic techniques, which are based on differences in the radiolucency of uncalcified epiphyses. Assessment of the maturation process relies on the detection of calcification nuclei and measurement of the thickness of the uncalcified cartilage of the growth plate.[1] This reflects the calcification progress of primary and secondary ossification centers.

The area between the calcified anlages of the primary and secondary nuclei of calcification contains several histologically distinct zones where enchondral ossification occurs.[2]

Aforementioned zones cannot be visualized using radiographic techniques. As different zones in the growth plate differ according to the degree of calcification and water content, they are magnetically susceptible and can be detected by MRI. Jaramillo et al.[3] used an experimental model and histological correlation to show that only T_1- and T_2-weighted pulse sequences obtained with a 1.5T scanner (GE Optima 360) allowed visualization of those layers as distinct morphological zones. They showed that physeal and epiphyseal cartilage presented distinct signal intensities; this opened the door for studies using signal postprocessing. A novel mathematical approach to signal interpretation—the statistical dominance algorithm (SDA)[4]—has been proposed to be able to delineate and possibly measure the areas showing signal differences.

The aim of this study was to evaluate different areas of the growth of plate using T_1- and T_2-weighted MR images, by implementing the SDA for the study of human radius in children.

Materials and Methods

This study was conducted in accordance with good medical practice outlines and was approved by the Ethics Committee of Jagiellonian University (permission no. 1072.6120.16.2017), and complied with the Declaration of Helsinki and good medical practice. Informed written consent for participation was obtained from the legal guardians of the examined children. We included the left hand of 10 healthy boys (age range 9–15 years), including two 9 years old, two 11 years old, three 12 years old, and two 15 years old without translation nor rotation between T_1-and T_2-weighted images. Presented patients' data were anonymized and described as P_{01}, P_{02}, …, P_{07}.

MR studies containing uncorrectable motion artifacts or that were technically imperfect were rejected. A 1.5T system (GE Optima 360, Chicago, IL, USA) with a dedicated four-channel wrist coil were used. T_1- and T_2-coronal plane sequences were applied. The following parameters were used to create T_2-weighted images: slice thickness, 3 mm; TR, 2749 ms; TE, 106 ms; number of averages, 2; spacing, 3.5 mm; echo train length, 23; bandwidth, 97 MHz. The following parameters were used to create T_1-weighted images: slice thickness, 3 mm; TR, 435 ms; TE, 16 ms; number of averages, 2; spacing 3.5 mm; echo train length, 23; bandwidth, 81 MHz. For the comparison of T_1- and T_2-weighted images, overlap of their condition of equal matrices had to be met (286 × 286 pixels matrices were used for the study).

[1]Department of Diagnostic Imaging, Jagiellonian University Medical College, 19 Kopernika Street, Cracow 31-501, Poland
[2]Department of Biocybernetics and Biomedical Engineering, AGH University of Science and Technology, Cracow, Poland

[*]Corresponding author, Phone: +48-12-424-7494,
E-mail: rafalobuchowicz@su.krakow.pl

Received: April 10, 2019 | Accepted: June 16, 2019

Growth plates were analyzed in coronal scans, separately, for the radius and ulna. The layers for the study were selected in the middle of the antero-posterior diameter of the examined epiphysis and therefore represented its widest part. Images were archived using a SIEMENS PACS (SYNGO, Siemens Healthineers, Erlangen, Germany). Anonymized studies were subsequently retrieved for mathematical postprocessing.

As the scanning time was relatively long (approximately 10 min for the whole study) and as the patients were children, an application test was compulsory. Using pixel-by-pixel positioning of the overlaid images, masks were developed that could compensate for the horizontal and vertical movements by a given number of pixels in case of minor movements. In the case of rotation, other transformations were applied.

Different luminance of the T_1- and T_2-weighted images was problematic. As the images from these sequences look quite similar, it was difficult to identify differences between the images reproducibly. Some of the images showed local changes in brightness, which hamper a uniform visualization of the differences between images, or comparison of different patients. Thus, T_1- and T_2-weighted images superposition required standardization.

Input image standardization

To standardize the superposition of T_1- and T_2-weighted images, we used a new image processing algorithm, the SDA, and its simplified version intended for image normalization, the statistical dominance transform (SDT).[5] The SDA transformation converts the image from the brightness domain to the domain of statistical information about dependencies of objects in the image. The algorithm essentially aims to determine the number of neighbors for each pixel in an area with a radius *R*. The resulting value is the number of pixels with a brightness greater than or equal to the brightness of the central pixel. The output image is a statistical indication of the dominance of points over their neighborhoods. The transformation is described by the code of SDA, as shown below:

```
for (x = N; x < SX - N; x++)
 for (y = N; y < SY - N; y++)
 {
  imgout[x, y] = 0;

  for (i = -N; i <= N; i++)
   for (j = -N; j <= N; j++)
    if  (i * i + j * j <= R * R)
      if (imgin[x + i, y + j] >=
              imgin[x, y] + threshold)
        imgout[x, y]++;
 }
```

where, imgin = input image (matrix), imgout = output image, *SX*, *SY* = width and height of input/output image, *R* = radius of neighborhood, *N* = size of neighborhood mask (also size of mirror margin used here), $N = \lceil R \rceil$, threshold = the threshold to be checked (especially for noisy images).

The SD transformation does not consider the additional threshold of dominance determination, which is assumed to be zero (SDA threshold = 0).

Such a procedure makes the picture independent of the dynamics of the luminance of the input image. As an example showing this key feature mentioned above, an analysis of the two different one-dimensional profiles could be provided (directional version assumed for simplicity) that have the same course (but not values) of valleys and peaks (Fig. 1A and 1B), thereby producing the same output from the algorithm (Fig. 1C and 1D, respectively).

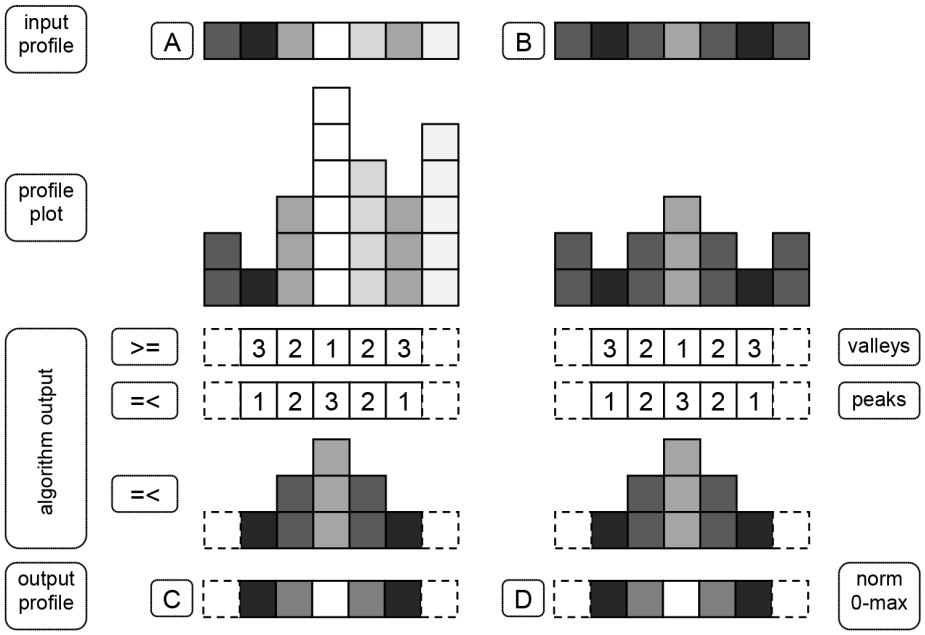

Fig. 1 An example of statistical dominance algorithm (SDA) normalization for one-dimensional images. Two different input profiles with the same course of valleys and peaks but different values, for radius $R = 1$ have the same output profiles. Margins were not considered to maintain clarity.

For this study, the value of the radius was assumed to be $R = 50$ pixels, because we found that further changes to the radius value did not result in significant changes. Radius selection is discussed in Fig. 6d in Nurzynska et al.[6]

Using the algorithm, the following goals were achieved:

(a) Input images are analyzed in a uniform way; irrespective of whether they differed in dynamics or resolution (e.g., 8 vs. 12 bit), important features are presented in the same way, allowing the interpretation to be standardized.
(b) Changes are emphasized, regardless of their brightness, making them easier to distinguish.
(c) Output images are standardized; each image is transferred to a new, strictly defined space, within a given range. Therefore, comparison of images is possible.

MR images subjected to SDA transformation (Fig. 2c and 2d) look very similar to the original images (Fig. 2a and 2b), while possessing features that allow further processing and analysis.

Superposition of T_1- and T_2-weighted images

To determine the resultant image, the difference in images after SDA transformation is calculated mathematically, as described by the following formula (1):

$$D_{\text{out}}[x,y] = (\text{SDA}(I_{T_1}))[x,y] - (\text{SDA}(I_{T_2}))[x,y] \qquad (1)$$

where, D_{out} = output matrix with difference values (superposition), $\text{SDA}(I_{T_1})[x, y]$ = pixel (x, y) values of SDA transformation applied on Image (T_1), $\text{SDA}(I_{T_2})[x, y]$ = pixel (x, y) values of SDA transformation applied on Image (T_2).

The differential image has positive values if the brightness of the objects in the T_1-weighted sequence is greater than the brightness of the objects in the T_2-weighted sequence; alternatively, the values are negative. A zero value means that both sequences have the same brightness.

Based on superposition outcomes of the transformed images, the following colors can be assigned to the corresponding areas:

- Source color (grayscale) indicates that T_1- or T_2-weighted images after SDA transformation have a value higher than 50% of the range, otherwise the following applied:
- Yellow indicates that the difference $D[x, y]$ is >0. The T_1-weighted image after the SDA transformation has a higher value than the T_2-weighted image after the transformation.
- Red indicates that the difference $D[x, y]$ is >0, and the value of the T_2-weighted image after transformation does not reach more than approximately 25% of the range.

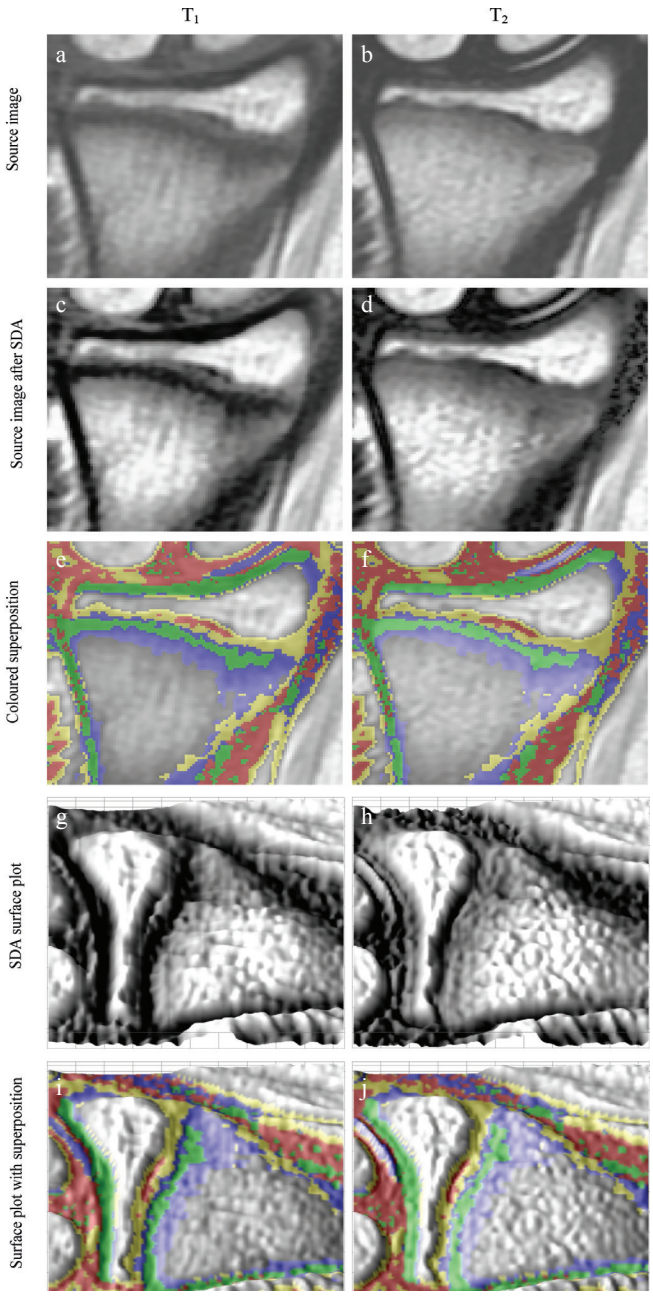

Fig. 2 The columns present transformation of T_1- and T_2-weighted source magnetic resonance images of patient P_{04}. (**a**) and (**b**) represents input images, T_1- and T_2-weighted images, respectively. (**c**) and (**d**) represents SDA transformation. (**e**) and (**f**) expresses colored signal differences based on superposition on T_1- and T_2-weighted images. (**g**) and (**h**) shows surface plots made on the basis of images transformed by applying the SDA. (**i**) and (**j**) shows colors representing signal differences overlaid on the surface plot of the normalized source images. SDA, statistical dominance algorithm.

- Blue indicates that the difference $D[x, y]$ is <0, and the T_2-weighted image after the SDA transformation has a higher value than the T_1-weighted image after the transformation.

- Green indicates that the difference $D[x, y]$ is <0, and the value of the T_1-weighted image after transformation does not reach more than approximately 25% of the range.

These descriptions are summarized in Table 1.

In the output obtained after image superposition using our proposed method, the zones of T_1- and T_2-weighted image value dominance were sharply delineated in the growth zones, in a repeatable, reproducible, and objective manners. T_1 image value dominance over T_2 image value was indicated in yellow and T_2 image value dominance over T_1 image value was indicated in blue color. The determination of the boundary between these zones of domination is free of the human factor. Based on the size and spacing of pixels in these color zones, the growth zone could be accurately measured. Moreover, subzones of markedly low brightness were considered. Low brightness areas in T_2-weighted images were marked in red color, visualized as separate spots on the yellow background (indicating general T_1 dominance). Low brightness areas in T_1-weighted images were marked in green color, visible as separate areas on the blue background (indicating general T_2 dominance). The thresholds for these subzones could be set manually, with a difference of ±3% from the initial threshold of 25%. Therefore, those zones were not used in isolation in growth zone measurement, as they were somewhat operator-dependent.

The obtained images were superimposed with special attention to pixel overlay in corresponding anatomical structures. Differences in the overlaid masks were highlighted where areas of non-mineralized zone with the highest volume of bounded and unbounded water were marked on the growth plate area on the image.

The colored regions obtained were used to determine the growth plate width. Based on pixel size and spacing in the particular image, the surface area was calculated, and the average thickness of the growth zones was was computed (pixel spacing of 0.293 mm). The data obtained are included in Table 2.

Table 1 Color projection of the differences in the image brightness recorded in human growth plates

Color	SDA(T_1), SDA(T_2) values of the range	T_1–T_2 difference	T_1 vs T_2
Source	SDA(T_1) > 50% OR SDA(T_2) > 50%	–	–
Yellow	SDA(T_1) ≤ 50% AND SDA(T_2) ≤ 50%	>0	$T_1 > T_2$
Red	SDA(T_1) ≤ 50% AND SDA(T_2) ≤ 25%		
Blue	SDA(T_1) ≤ 50% AND SDA(T_2) ≤ 50%	<0	$T_1 < T_2$
Green	SDA(T_1) ≤ 25% AND SDA(T_2) ≤ 50%		

SDA, statistical dominance algorithm.

Results

Using the SDA, we were able to show repeatedly that the zones in the growth plate of bone could be indicated by different colors (Fig. 3). These differences represent the dominance of the signal arising from the T_1 and T_2 pulse sequences. As these color differences represent areas with markedly different water content, we assumed that this technique allowed distinction of the distribution of different histological areas in the growth plate (Fig. 3). This idea might be supported by the observation of the color zone distribution in the growth plates of children of different ages (Fig. 4). The wrist of a 9-year-old child presented a significantly broader green area than seen in the wrist of a 12-year-old child. This green area represents the higher T_2-weighted image brightness than T_1-weighted image, and is indicative of watery cartilage. This area was not present in a 15-year-old subject. The yellow area

Table 2 Width of growth zone areas estimated on the basis of pixel counts in the different growth plate zones

Years old	Patient ID	$T_2 > T_1$	$T_1 > T_2$
		B + G (mm)	R + Y (mm)
11	P_{02}	1.81	0.77
	P_{03}	1.98	0.78
12	P_{04}	3.69	1.27
	P_{05}	3.53	1.72
	P_{06}	3.52	1.49

B + G means blue + green zone width and R + Y means red + yellow zone width.

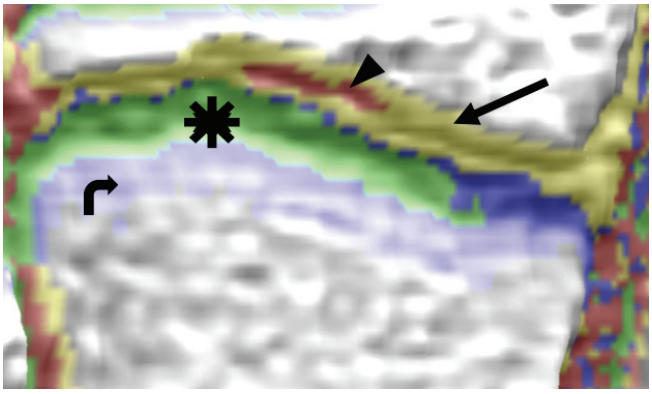

Fig. 3 High signals in T_2-weighted sequences reflect epiphyseal and physeal cartilage zone distribution (reflected by zones in blue and green color—curved arrow and asterisk, respectively). The more distal area of higher T_1 signals is represented by a yellow color that reflects the zone of provisional calcification (arrow). The arrowhead represents the area of marked T_1 signal dominance.

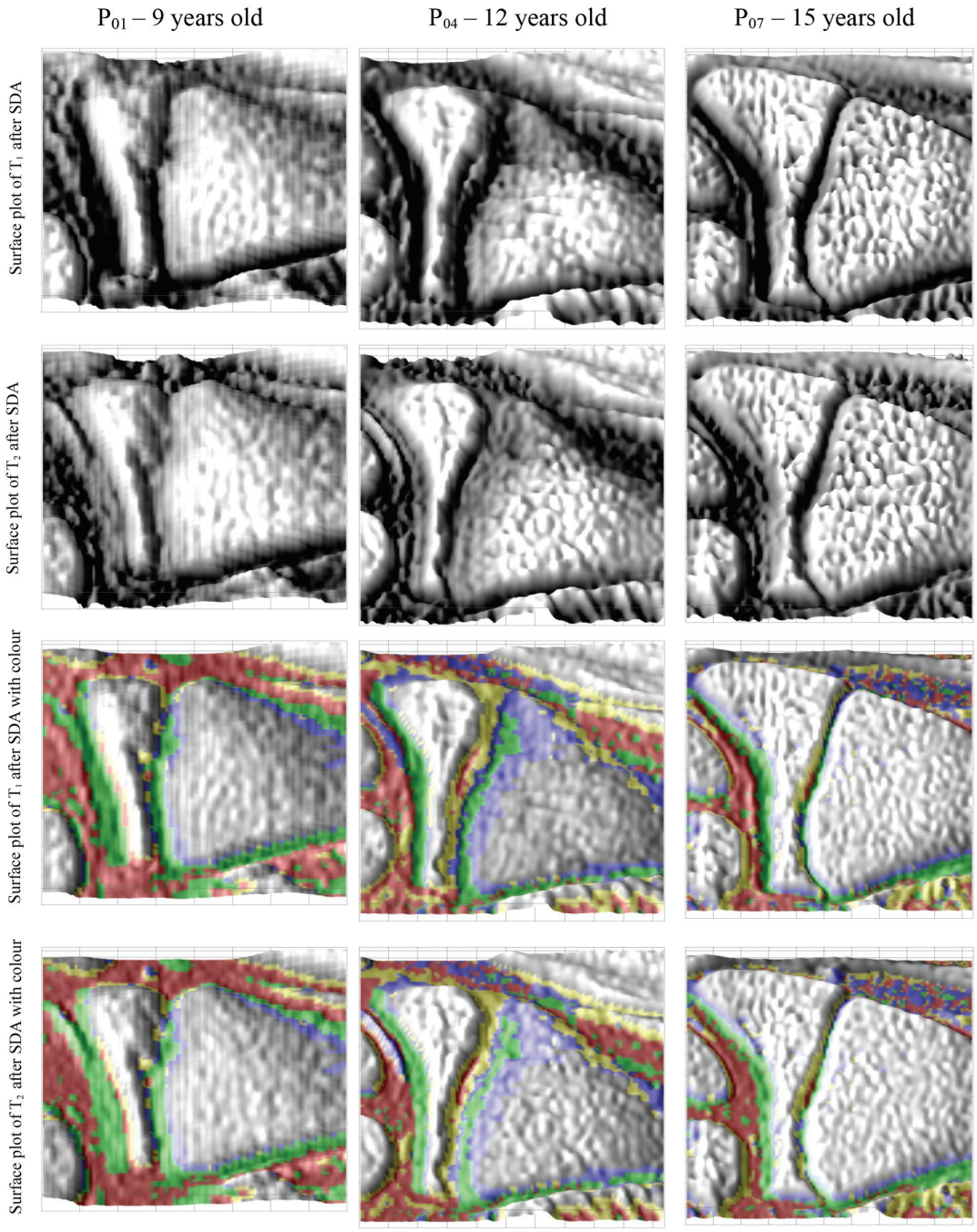

Fig. 4 Surface plots of the T_1- and T_2-weighted magnetic resonance images of the wrists after SDA transformation with superimposed colors representing signal differences in the area of the growth plate of 9-, 12-, and 15-year-old children. Note the changes in the growth plate and the color distribution in the patients of different age. SDA, statistical dominance algorithm.

represents a high T_1-weighted image area that reflects the presence of a provisional calcification zone, and was broader in 12-year-old patients than in 9-year-old patients. In 15-year-old patients, this area was dominant and reflects the ongoing maturation of the physis (Fig. 4).

Mapping of the different signal intensity distributions across growth plates was reproducible in the group of one 11-year-old, and two 12-year-old subjects, as shown in Fig. 5. The proximal high signal zone, indicated in green, represents area of hydrated tissue with a high signal intensity in T_2-weighted images; the yellow distal part represents the tissue of the calcification zone, which contains less water.

The proposed method of normalization allows to compare T_1- and T_2-weighted images with different

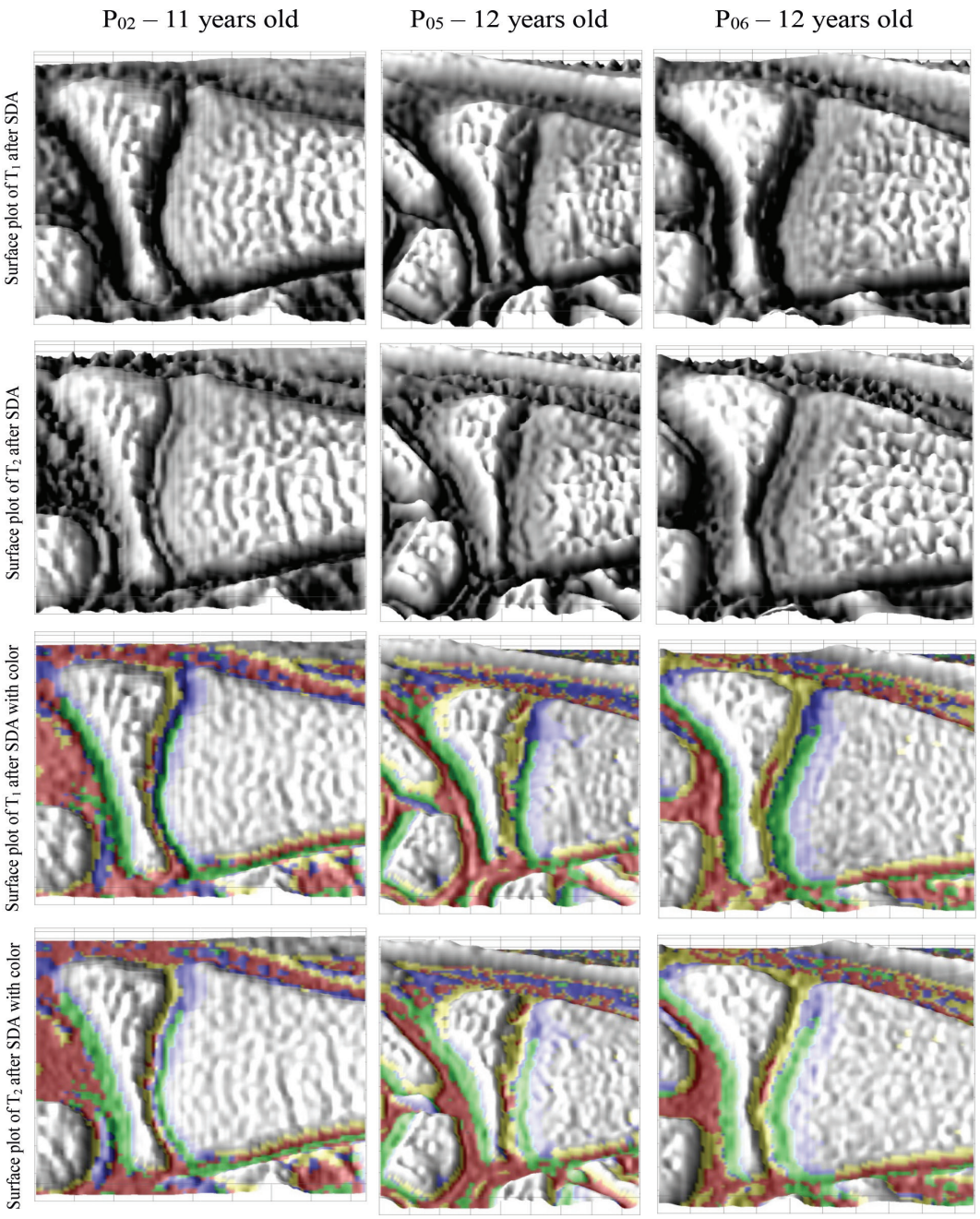

Fig. 5 Distribution of the colors representing different water content in the area of the growth plate in an 11 to 12-year-old patient. Note the similarities of the distribution of the green areas (proximal), which represents high water content (T_2-weighted image brightness dominance), and distal yellow areas, which represents low water content (T_1-weighted image dominance).

illumination (Fig. 6, T_1 source values are dominating over T_2 source values; seen as a red line of profile). The comparison of different superposition outputs for source images and normalized outputs for SDA transformed images is presented in Fig. 7. It shows that using SDA as normalization method the high reproducibility of ROI pattern was achieved, in opposite to unnormalized source image.

Discussion

Radiographic technique based bone age assessment is the most accepted and widely used approaches for estimation of bone age in pediatric populations.[7] Much effort has been expended to develop methods that allow automatic evaluation of radiographic images by means of computerized graphic analysis.[8] The BoneExpert software described by Martin et al.[9]

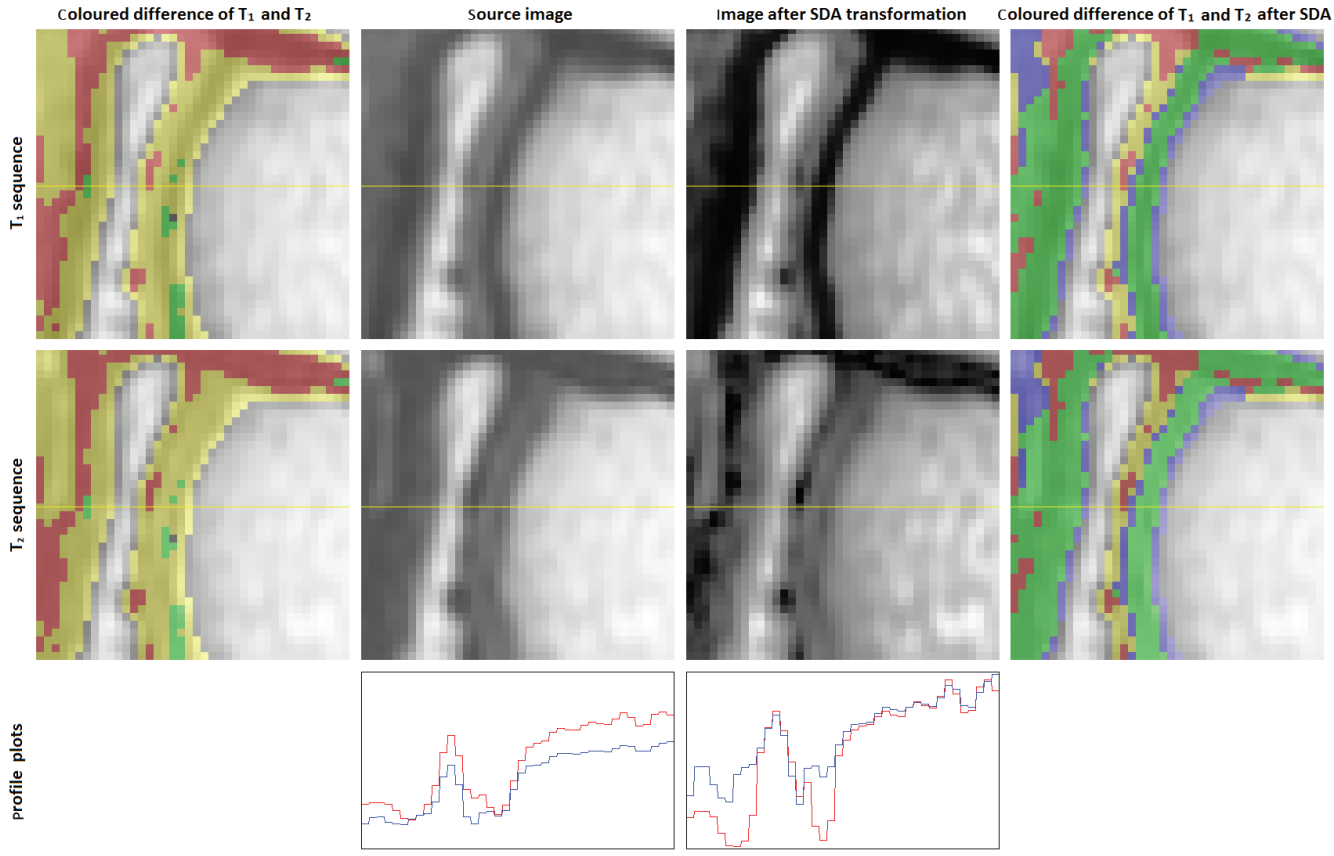

Fig. 6 Profile plots for superposition on source input data and SDA-transformed input data. Red line represents T_1 values and blue T_2 values. SDA, statistical dominance algorithm.

is a system that can generate shapes and appearances based on bone recognition from a radiographic image and was reported to have high precision in both boys and girls. All aforementioned techniques were based on X-ray techniques that are potentially hazardous for young patients. Therefore, new techniques were sought among more acceptable radiological modalities, i.e., ultrasonography and MRI.

Utilization of MRI in this respect involves two different ways of utilizing MR images for assessing calcification nuclei, as in radiography, but without the hazardous ionizing radiation, as proposed by George et al.[10] Classic radiography overrates the maturity of the epiphyses, while MR is much more precise in assessing the presence of chondrous tissue between nuclei of ossification. The concept of utilizing MR for rating bone maturity was later developed by Terada et al.,[11] who used a gradient echo 3D sequence; segmentation and normalization was able to validate the method in comparison with standard radiographic atlases.

In the current study, we proposed a novel approach for analyzing bone maturity based on the morphology of the growth plate using T_1- and T_2-weighted pulse sequences. Analysis of uncalcified growth plate width as a whole was implemented with a focus on the chondrous "watery" layer as the part in which growth and development occurs. This advances the concepts of Dvorak et al.[12] who analyzed and graded the fusion of the growth plate based on T_1-weighted scans of the radii of football players and compared the results obtained with plain radiographs. The approach presented in our work differs from these studies, in that we attempted to evaluate the width of the growth plate precisely. Application of algorithms developed in this study allowed us to extract precisely the features of the uncalcified zone of the growth plate, representing the area of chondroprogenitors and proliferating cells, as described by Hochberg.[2] To the best of our knowledge, our work is the first attempt to delineate precisely and directly measure uncalcified growth plate in the basis of the signal differences in the MR pulse sequences.

Our study had some limitations. Histological verification of our finding was not possible in the current model for ethical reasons, but we plan to continue this further in a cadaveric study. Additionally, we used a small group of patients. Nevertheless, this preliminary study illustrated the feasibility of extracting chondrous tissue from MR images with this technique; it should be further verified in a larger group of patients. An error in the segmentation of the growth plate has to be taken into account, given the small area of interest and the averaging effect due to

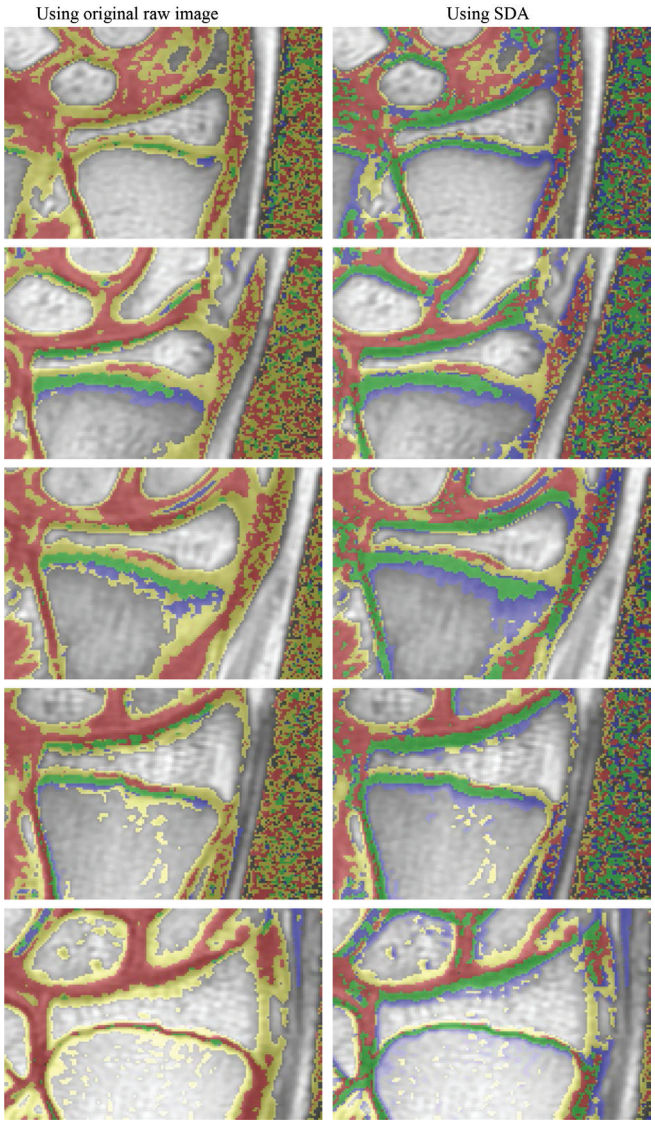

Fig. 7 Comparison of T_1- and T_2-weighted image superposition for source images and transformed images for five patients – reproducibility of pattern for normalized images. SDA, statistical dominance algorithm.

different proportions of water, proteoglycans, and collagen in the analyzed tissue. Further studies are needed to evaluate this problem.

Conclusion

Using our method, we were able to develop new indexes describing the size of the uncalcified layer, expressed as ratio of diameter of uncalcified epiphyseal area vs. growth plate area. This approach might be clinically useful, because it utilizes only two sequences, namely T_1- and T_2-weighted images, which are short and available in all MR systems. The SDA method applied in this study is used in a program that allows reproducible normalization to a standardized threshold across all examined studies as opposed to operations on source data (Fig. 6). This allows the use of MR images for further comparative analyses and extraction of non-calcified areas of different intensity that represent the different areas of the growth plate. This could facilitate detection of lesions in the growth plate by means of MRI.

Ethical Statement

All procedures performed in studies involving human participants were in accordance with the ethical standards of the institutional and national research committee and with the 1964 Helsinki declaration and its later amendments or comparable ethical standards.

Informed Consent

Informed consent was obtained from the legal guardians of all individual participants included in the study.

Funding

This research did not receive any specific grant from funding agencies in the public, commercial, or not-for-profit sectors.

Acknowledgment

We thank W. Guz, MD, PhD, for his assistance in data acquisition.

Conflicts of Interest

The authors declare no conflicts of interest.

References

1. Cameriere R, Ferrante L, Mirtella D, Cingolani M. Carpals and epiphyses of radius and ulna as age indicators. Int J Legal Med 2006; 120:143–146.
2. Hochberg Z. Clinical physiology and pathology of the growth plate. Best Pract Res Clin Endocrinol Metab 2002; 16:399–419.
3. Jaramillo D, Laor T, Zaleske DJ. Indirect trauma to the growth plate: results of MR imaging after epiphyseal and metaphyseal injury in rabbits. Radiology 1993; 187:171–178.
4. Piórkowski A. A statistical dominance algorithm for edge detection and segmentation of medical images, In: Piętka E, Badura P, Kawa J, Wieclawek W, eds. Advances in Intelligent Systems and Computing, Information Technologies in Medicine, Springer, Cham, 2016; 3–14.
5. Kociołek M, Piórkowski A, Obuchowicz R, Kaminski P, Strzelecki M. Lytic region recognition in hip radiograms by means of statistical dominance transform, In: Chmielewski L, Kozera R, Orłowski A, Wojciechowski K, Bruckstein A, Petkov N, eds. Computer Vision and Graphics. ICCVG 2018. Lecture Notes in Computer Science, vol 11114. Springer, Cham, 2018; 349–360.

6. Nurzynska K, Mikhalkin A, Piorkowski A. CAS: Cell Annotation Software - Research on neuronal tissue has never been so transparent. Neuroinformatics 2017; 15:365–382.
7. Satoh M. Bone age: assessment methods and clinical applications. Clin Pediatr Endocrinol 2015; 24:143–152.
8. Sato K, Ashizawa K, Anzo M, et al. Setting up an automated system for evaluation of bone age. Endocr J 1999; 46: S97–S100.
9. Martin DD, Sato K, Sato M, Thodberg HH, Tanaka T. Validation of a new method for automated determination of bone age in Japanese children. Horm Res Paediatr 2010; 73:398–404.
10. George J, Nagendran J, Azmi K. Comparison study of growth plate fusion using MRI versus plain radiographs as used in age determination for exclusion of overaged football players. Br J Sports Med 2012; 46:273–278.
11. Terada Y, Kono S, Uchiumi T, et al. Improved reliability in skeletal age assessment using a pediatric hand MR scanner with a 0.3T permanent magnet. Magn Reson Med Sci 2014; 13:215–219.
12. Dvorak J, George J, Junge A, Hodler J. Application of MRI of the wrist for age determination in international U-17 soccer competitions. Br J Sports Med 2007; 41:497–500.